

## WALL-MODELED LARGE-EDDY SIMULATIONS OF SHOCK/TURBULENT-BOUNDARY-LAYER INTERACTIONS IN A LOW ASPECT-RATIO DUCT

**Iván Bermejo-Moreno**

Center for Turbulence Research  
Stanford University, Stanford, CA 94305, USA  
ibermejo@stanford.edu

**Laura Campo**

Department of Mechanical Engineering  
Stanford University, Stanford, CA 94305, USA  
lcampo@stanford.edu

**Johan Larsson**

Center for Turbulence Research  
Stanford University, Stanford, CA 94305, USA  
Currently at: Department of Mechanical Engineering  
University of Maryland, College Park, MD 20742, USA  
jola@umd.edu

**Julien Bodart**

Center for Turbulence Research  
Stanford University, Stanford, CA 94305, USA  
jbodart@stanford.edu

**David Helmer**

Department of Mechanical Engineering  
Stanford University, Stanford, CA 94305, USA  
dhelmer@stanford.edu

**John K. Eaton**

Department of Mechanical Engineering  
Stanford University, Stanford, CA 94305, USA  
eatonj@stanford.edu

### ABSTRACT

We present large-eddy simulations of the interaction of an oblique shock wave impinging and reflecting off a turbulent boundary layer in a nearly-square duct. A small compression wedge spanning the top wall of the duct deflects the incoming air stream ( $M = 2.05$ ) generating a shock wave that interacts with the bottom wall turbulent boundary layer. The simulations incorporate an equilibrium wall model aimed at reproducing the moderately high Reynolds numbers of the boundary layer under consideration ( $Re_\theta \approx 6,500$ ). Simulation results are first validated by comparison with experimental PIV data (Helmer *et al.*, 2012; Campo *et al.*, 2012) of mean and turbulence quantities taken in planes near the center of the duct and near the side walls. Two different strengths of the incident shock wave are considered, corresponding to increasing heights of the compression wedge. Planes perpendicular to the PIV measurements are then extracted from the simulations to complement experimental findings related to the three-dimensionality imposed by the side walls. In particular, the downstream evolution of corner flows is explored.

### INTRODUCTION

The interaction of an oblique shock wave impinging upon and reflecting from a turbulent boundary layer is relevant in the efficient design of isolators for air-breathing supersonic engines, among other applications. Despite the large body of experiments (see, for example, Dolling, 2001; Dupont *et al.*, 2006, 2008; Humble *et al.*, 2009; Souverein *et al.*, 2010) and numerical simulations, both DNS (Wu & Martin, 2008; Pirozzoli & Grasso, 2006) and LES (Gar-

nier *et al.*, 2002; Touber & Sandham, 2009), found in the fluid mechanics literature, open questions remain, such as the origin of large-scale low-frequency motions (Pirozzoli *et al.*, 2010; Priebe & Pino Martin, 2012; Grilli *et al.*, 2012) and the three-dimensionality of the flow features resulting from the presence of side walls. Recent experiments performed by Helmer *et al.* (2012) and Campo *et al.* (2012) were designed specifically to address the latter by using a wind-tunnel with a low-aspect ratio cross-section and taking PIV measurements in planes near the side wall, in addition to a near-center plane. Numerical simulations are often performed with periodic transverse boundaries, missing any three-dimensional effects that would result from the side walls found in several engineering configurations.

The high Reynolds numbers typically achieved in experiments targeting realistic flow conditions make unfeasible the use of direct numerical simulations (DNS) or even large-eddy simulations (LES), due to the small scales structures that need to be resolved in the turbulent boundary layers that form near the walls. A compromise is often made by simulating the flow at a lower Reynolds number and extrapolating the results to higher Reynolds numbers. An alternative is to use a wall model to avoid having to resolve the inner-most region of the turbulent boundary layer, thus lowering the mesh resolution requirements of the simulation.

The present work aims to perform wall-modeled large-eddy simulations (WMLES) of the interaction of oblique shocks of different strengths with a turbulent boundary layer in a low-aspect-ratio duct. The simulations target the experimental conditions of Helmer *et al.* (2012) and are extended to stronger interactions for which experiments are

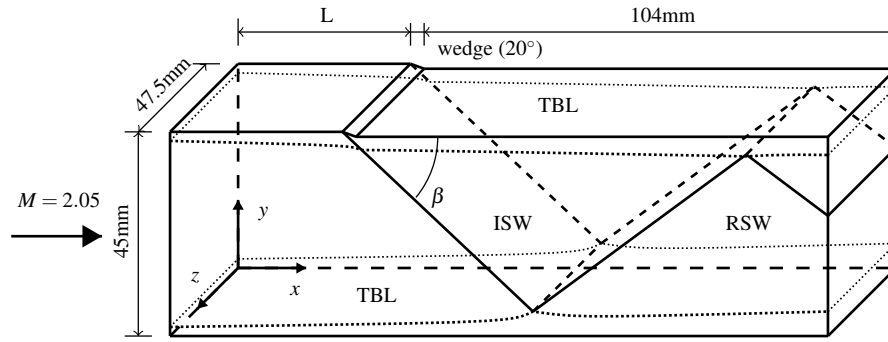


Figure 1. Computational setup: M, Mach number; TBL, turbulent boundary layers (only top and bottom drawn, for clarity); ISW, incident shock wave; RSW, reflected shock waves.

currently being performed in parallel to this computational effort. The objective is to assess whether LES using a purely equilibrium wall model can predict boundary layer flows that are clearly out of equilibrium, such as the rapid deceleration occurring in the SBLI and the stress-induced secondary flows present in the duct corners. Comparison with experimental PIV data retrieved in planes parallel to the side walls will be shown for validation.

## FLOW CONDITIONS AND COMPUTATIONAL SETUP

The computational domain (see figure 1) replicates part of the test section of the continuously operated Mach 2.05 wind tunnel used in the experiment (Helmer *et al.*, 2012), fed from a 2D converging/diverging nozzle followed by a constant-area development section of 45 mm  $\times$  47.5 mm. A small 20° compression wedge spans the top wall of the duct and generates an oblique shock that impinges and reflects at the bottom wall. Another constant-area section is located downstream of the compression wedge.

Presently, two wedge configurations are considered, corresponding to heights of 1.1 mm and 3 mm. The computational domain for each configuration extends 21 mm and 37 mm, respectively, upstream of the wedge foot, taken as the origin of the streamwise coordinate,  $x$ . A larger wedge translates into a stronger oblique shock and, therefore, a stronger interaction with the boundary layer. The length of the duct that follows the contraction is 104 mm in both computational configurations. A boundary layer thickness of  $\delta_0 = 5.4$  mm measured in the experiment on the top wall 21 mm upstream of the foot of the wedge will be considered as a reference length scale. The Reynolds number based on the momentum thickness of the incoming boundary layer at that measurement location is  $Re_\theta \approx 6,500$ , with a center line velocity of approximately 525 m/s.

The simulations are performed using the control-volume-based, finite-volume solver of the spatially filtered, compressible Navier-Stokes equations on unstructured grids, *Charles<sup>X</sup>*, developed at the Center for Turbulence Research. It employs a third-order Runge-Kutta time discretization and a grid-based blend of non-dissipative central and dissipative upwind fluxes. It utilizes Vreman's sub-grid scale model (Vreman, 2004) and an ENO shock-capturing scheme, active only in regions where the negative rate of dilatation,  $-\partial_j u_j$ , is larger than  $\max(\sqrt{\omega_j \omega_j}, 0.1c/h)$ , where  $\omega_j$  is the vorticity,  $c$  the sound speed and  $h$  the cell (control volume) size. The sub-grid

scale model is not applied in regions where shock-capturing is active, to avoid adding more numerical dissipation to the already dissipative ENO scheme. We use the equilibrium wall model proposed by Kawai & Larsson (2012), outlined later in this section.

Independent simulations on three meshes with increased resolution are performed for each geometric configuration, as part of a grid-convergence study. Meshes include approximately 4.5 (5), 18 (20) and 36 (40) million control volumes, respectively, for the 1.1 mm (3 mm) wedge height case. For each mesh, the grid spacing in the streamwise direction is kept uniform (with  $\Delta x/\delta_0 = 1/10, 1/16$  and  $1/20$ , for increasing resolution). In each transverse direction ( $\eta = y, z$ ) the grid stretches from the walls (where  $\Delta \eta/\delta_0 = 1/70, 1/105$  and  $1/135$  for increasing mesh resolution) up to a distance of  $2\delta_0$ , remaining uniformly spaced in the core and equal to the streamwise grid spacing.

The inflow boundary condition for the numerical simulations is produced by a synthetic turbulence generator, following the method of Touber & Sandham (2009). This algorithm is based on the digital filtering technique proposed by Klein *et al.* (2003) and is designed to match specified single- and two-point correlations. One-dimensional profiles of mean velocities and Reynolds stresses, taken from experimental PIV measurements at probes located 2.5, 4.0, 5.5 and 21 mm from the side wall and at the streamwise location of the computational inlet are mapped, through symmetries and anti-symmetries, to create a two-dimensional inflow. The pressure at the inlet is assumed constant (at the wall measured value of  $p = 33,100$  Pa measured in the experiment). The one-dimensional mean temperature profiles are approximated from the mean velocity profiles using the Crocco-Busemann relation with a recovery factor of 0.89. The imposed turbulence length scales at the inflow are  $\delta_0$  in the streamwise coordinate and  $\delta_0/2$  in the transverse directions.

## Wall model

We use the wall model proposed by Kawai & Larsson (2012), in which the equilibrium-boundary-layer equations are solved in a refined, near-wall inner grid, embedded in the coarser, outer LES grid:

$$\frac{d}{d\eta} \left[ (\mu + \mu_t) \frac{du_{\parallel}}{d\eta} \right] = 0 \quad (1)$$

$$\frac{d}{d\eta} \left[ (\mu + \mu_t) u_{\parallel} \frac{du_{\parallel}}{d\eta} + c_p \left( \frac{\mu}{Pr} + \frac{\mu_t}{Pr_t} \right) \frac{dT}{d\eta} \right] = 0. \quad (2)$$

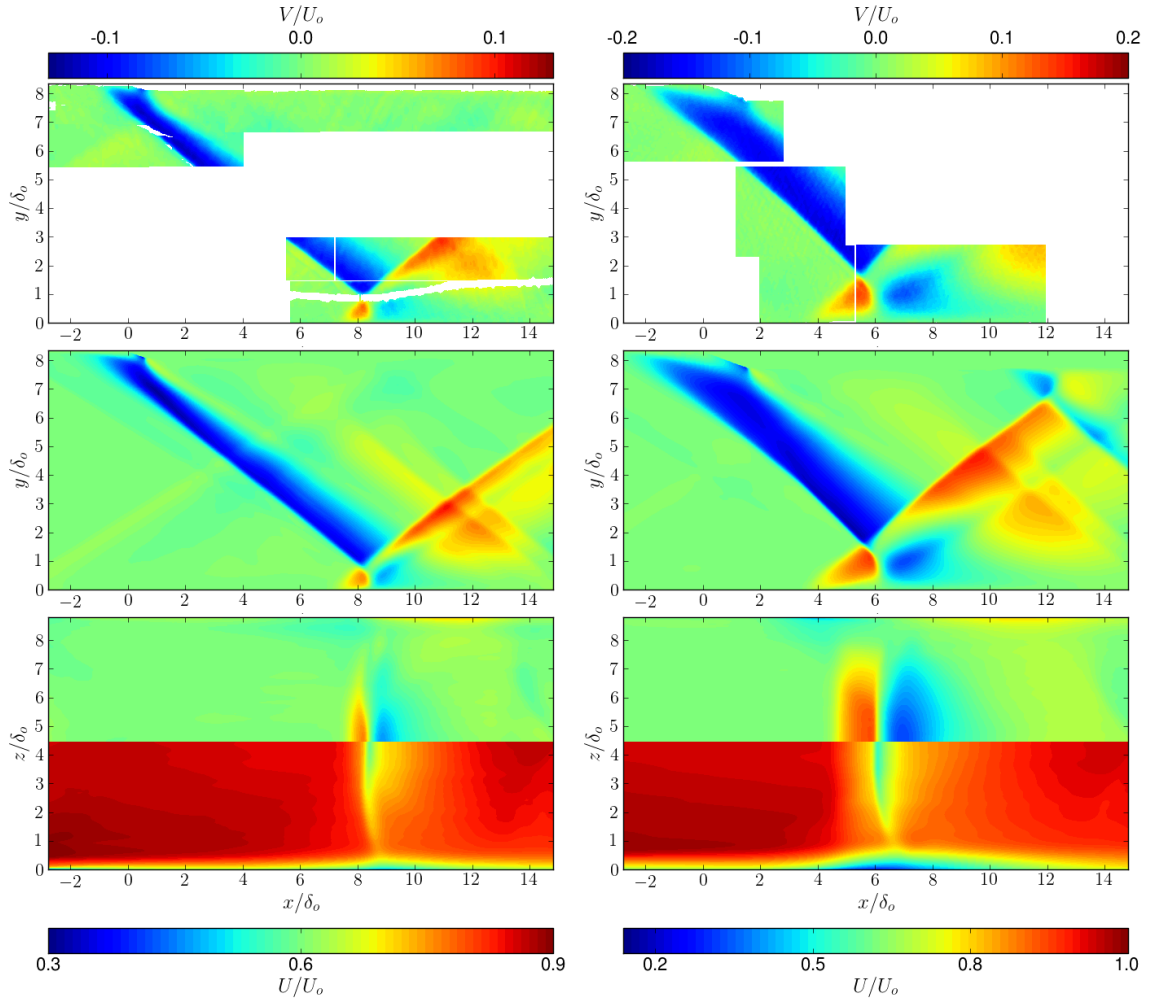


Figure 2. PIV (top) and LES (central) mean vertical velocity contours at a near-center plane ( $z/\delta_o = 3.89$ ) for the interactions produced by the compression wedge of height 1.1 mm (left) and 3 mm (right). The bottom plot includes contours of mean vertical velocity (upper half) and mean streamwise velocity (lower half) in a horizontal ( $xz$ -) plane taken at a distance from the bottom wall of approximately half the height of the crossing point between the incident and reflected shock waves, for each interaction case. Blank regions in the PIV data (top) correspond to unavailable experimental measurements.

$\eta$  is the wall-normal coordinate,  $u_{\parallel}$  is the wall-parallel velocity,  $T$  is the temperature,  $c_p$  is the fluid-specific heat capacity at constant pressure,  $\mu$  is the fluid molecular viscosity,  $Pr$  is the Prandtl number and  $\mu_t$  is the wall-model eddy-viscosity, which is taken from a mixing-length model as

$$\mu_t = \kappa \rho \eta \sqrt{\tau_w / \rho} \left[ 1 - \exp\left(-\frac{\eta^+}{A^+}\right) \right]^2, \quad (3)$$

where  $u_{\tau} \equiv \sqrt{\tau_w / \rho_w}$  is the friction velocity based on the wall shear stress,  $\tau_w$ , and wall density,  $\rho_w$ .  $\eta^+ \equiv \rho_w u_{\tau} \eta / \mu_w$  is the wall-normal coordinate normalized to viscous units. The model parameters are set constant:  $\kappa = 0.41$ ,  $Pr_t = 0.9$ ,  $A^+ = 17$ .

The inner wall-model simulation takes the LES flow variables ( $\rho, u, T$ ) as boundary condition at a specified wall-normal distance,  $h_{wm}$ . In the present simulations we use  $h_{wm}/\delta_o = 0.06$ ; note that this distance is fixed independent of the computational mesh, as proposed by Kawai & Larsson (2012). The LES takes the wall-shear stress and heat-flux at the wall,  $\tau_w$  and  $q_w$ , respectively, from the wall-

model inner simulation. The wall model is applied in all four walls of the LES, considered adiabatic.

## RESULTS

The mean flow features near the center plane of the duct ( $z/\delta_o = 3.89$ ) are qualitatively well reproduced by the LES results, when compared with the PIV experimental measurements, as shown in the top and central plots of figure 2. The location, extension and shape of the shock/boundary-layer interaction (SBLI) occurring at the bottom wall match the experimental results for both the 1.1 and 3 mm wedge heights. For the two incident shock strengths, the region perturbed by the SBLI at the top wall (produced by the compression wedge) extends slightly further upstream in the simulation than in the experiments.

The side walls strongly affect the bottom-wall SBLI (see bottom plots in figure 2). For the 1.1 mm-high wedge (left plots) the strength of the SBLI interaction rapidly decreases at distances over  $\delta_o$  away from the center-plane. The shock front curves downstream as it gets closer to the side walls, also thickening their boundary layers near the

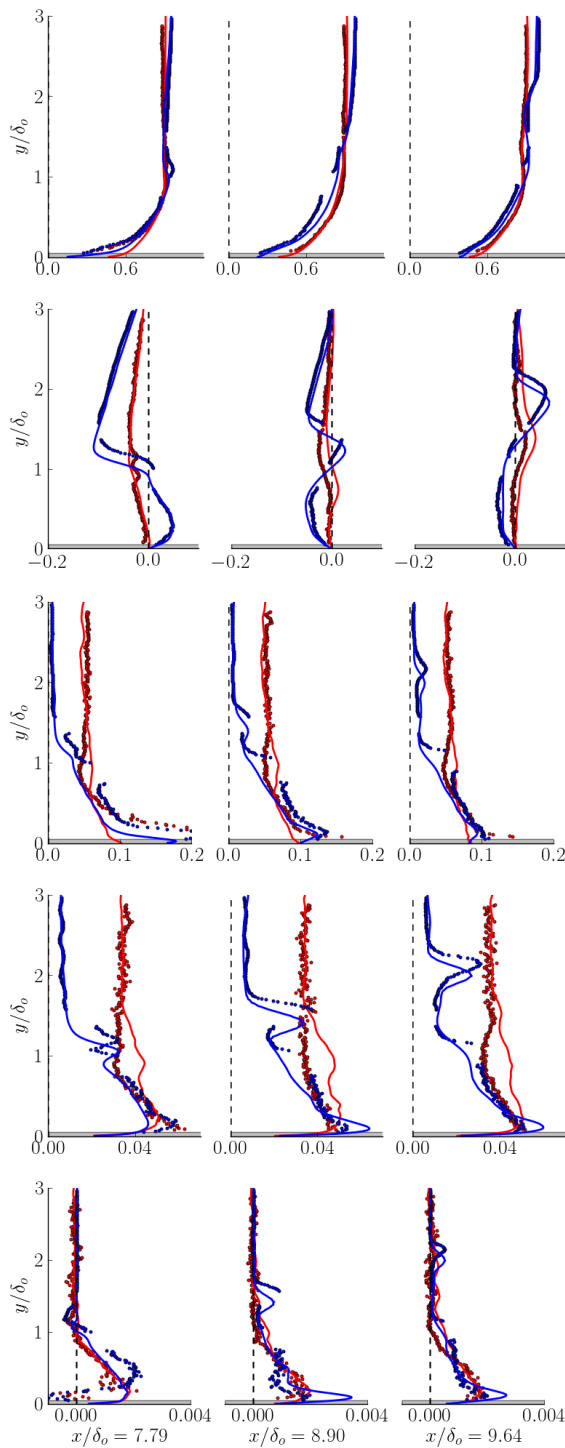


Figure 3. Vertical profiles of  $U/U_o$ ,  $V/V_o$ ,  $u'/U_o$ ,  $v'/U_o$ ,  $-u'v'/U_o^2$  (top to bottom), at three streamwise locations (left to right), for the 1.1 mm-high wedge reflected SBLI. Dots: PIV, lines: LES. Blue: near-center plane ( $z/\delta_o = 3.89$ ), red: near-side wall plane ( $z/\delta_o = 0.74$ )

of the shock/wall impingement, as it is observed in the lower half of the bottom plots in figure 2, corresponding to the streamwise velocity contours. The stronger interaction, corresponding to the 3 mm-high wedge case, shows a wider thickening effect of the lateral boundary layers, and the nearly two-dimensional interaction region in the duct

core extends further towards the side walls, when compared with the 1.1 mm-high wedge case.

A more quantitative analysis of the LES results, in comparison with PIV measurements, is presented in figures 3 and 4, for the 1.1 and 3 mm-high wedge cases, respectively, including turbulence quantities (streamwise,  $u'$ , and vertical,  $v'$ , velocity fluctuations, as well as Reynolds shear stress,  $u'v'$ ) in addition to the mean streamwise and vertical velocities ( $U$  and  $V$ , respectively). The shaded areas in those figures correspond to the extension of the wall-model inner grid, near the bottom wall ( $y/\delta_o < 0.06$ ). The spanwise location of the two planes for which profiles are shown correspond to  $z/\delta_o = 3.89$  (near the duct center) and  $z/\delta_o = 0.74$  (near the side wall), with profiles shown in blue and red, respectively.

For the 1.1 mm wedge (figures 3), mean streamwise and vertical LES velocity profiles are in good agreement with PIV data, although the vertical extent of the SBLI seems to be underpredicted by approximately  $0.1\delta_o$ . Close to the bottom wall, the streamwise velocity profiles are fuller in the simulation, particularly in the most upstream locations shown, likely corresponding to a more developed turbulent boundary layer than in the experiment. The strength of the interaction when approaching the side wall is decreased (red curves), which translates into more uniform mean streamwise velocity profiles for the three locations and also flatter vertical velocity profiles. For the latter, the agreement is best at the most upstream location plotted, whereas the LES overestimates the mean vertical deflection downstream.

Turbulence quantities—streamwise and vertical velocity fluctuations,  $u'$  and  $v'$ , and Reynolds shear stress,  $u'v'$ —show reasonable agreement with PIV measurements. In both planes considered, the constant experimental values in the inviscid region (i.e.,  $y/\delta_o \gtrsim 1.8$  away from the bottom wall) are accurately reproduced in the LES. Peaks of vertical velocity fluctuations,  $v'$  in the near-center plane (blue curves), which correspond to the turbulence amplification produced by the interaction with the incident/reflected shocks, show offsets consistent with a slightly thinner ( $\approx 0.1\delta_o$ ) SBLI obtained in the LES, compared with the experiment. For the near-side wall profiles, the LES overpredicts  $v'$  below  $y/\delta \approx 1.5$ , recovering the correct value near the wall. At the most upstream location, the LES underpredicts the  $u'$  near the bottom wall ( $y/\delta_o \lesssim 0.5$ ).

For the 3 mm-high wedge configuration (figure 4), mean streamwise and vertical LES velocity profiles are generally in good agreement with PIV data, accurately predicting the streamwise and vertical sizes of the interaction in both near-center and near-side-wall planes. Fuller streamwise velocity profiles at the most upstream location are nevertheless observed for  $y/\delta_o < 0.15$ . These appear to translate into higher values of the streamwise and vertical velocity fluctuations in the PIV, which are underpredicted in the LES below  $y/\delta_o \approx 0.5$ . At the core of the SBLI interaction region, for the near-center plane (blue curves in the center plots of figure 4) the streamwise and vertical velocity fluctuations are underpredicted in the LES, even though the shape of the profiles and the location of the peaks matches those of the experiment. Downstream (right plots) the turbulence quantities in the near-center plane show good agreement with the PIV. In the near-side-wall plane (red curves), the inviscid values of streamwise and vertical velocity fluctuations are overpredicted in the LES, indicative of a thicker side-wall boundary layer in the LES at that location.

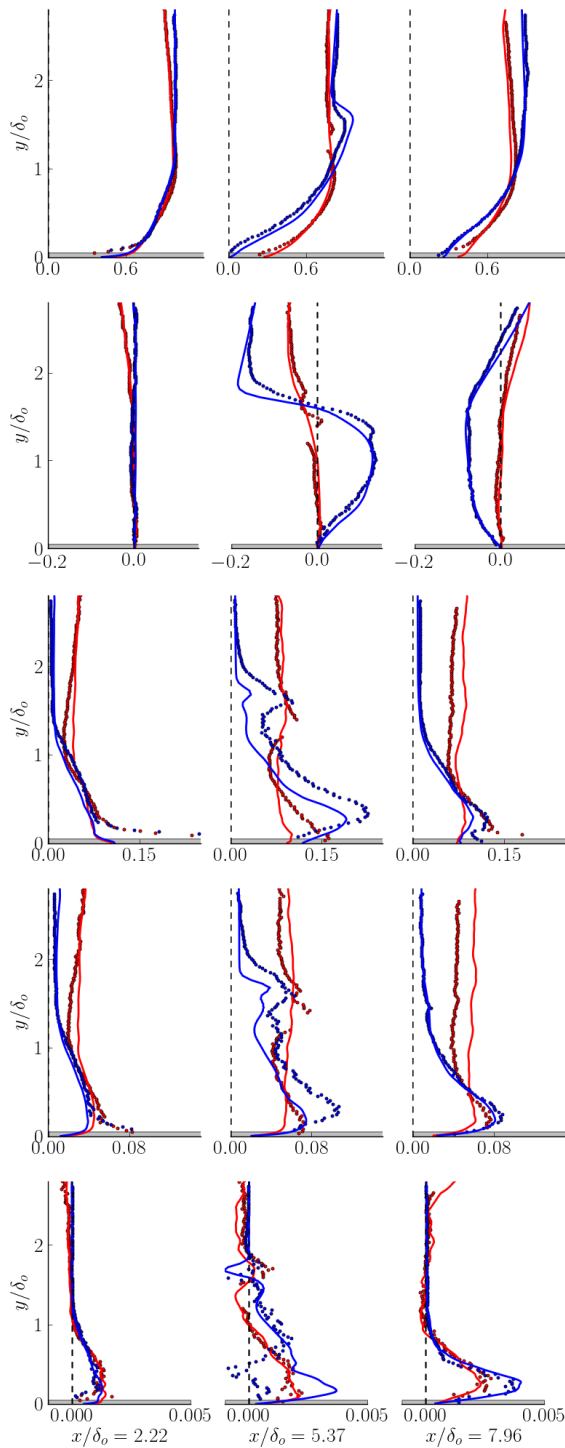


Figure 4. Vertical profiles of  $U/U_o$ ,  $V/V_o$ ,  $u'/U_o$ ,  $v'/U_o$ ,  $-u'v'/U_o^2$  (top to bottom), at three streamwise locations (left to right), for the 3 mm-high wedge reflected SBLI. Dots: PIV, lines: LES. Blue: near-center plane ( $z/\delta_o = 3.89$ ), red: near-side wall plane ( $z/\delta_o = 0.74$ )

### Corner flows

Gradients of Reynolds stresses present near the corners of the duct induce streamwise vorticity, resulting in secondary flows of Prandtl's second kind (see Bradshaw, 1987; Gessner, 1973). These secondary flows consist of a pair of counter-rotating vortices located in each corner of the duct.

Besides the motion induced in the cross-sectional planes, corner flows also result in a modification of the streamwise velocity flow. Experimental studies exist for supersonic flows in square ducts (Gessner *et al.*, 1987; Davis *et al.*, 1986) at a higher Mach number than the present work.

LES results confirm the presence of such corner flows for the current configuration and allow the investigation of the corresponding downstream evolution as they interact with the shock waves. Figure 5 shows mean streamwise velocity contours at the  $y = z = 0$  corner (bottom wall), with arrows superimposed that represent mean transverse velocity. Results for the 1.1 mm-high wedge height case are shown at three streamwise locations.

The left plot of figure 5 shows the unperturbed corner flows at a cross section of the duct located  $6\delta_o$  upstream of the reflected SBLI shock-crossing point (see figure 2 for reference). A nearly symmetric pair of elliptical counter-rotating vortices can be seen, with cores located at  $(y,z) \approx (0.25\delta_o, 0.1\delta_o)$  and  $(y,z) \approx (0.1\delta_o, 0.25\delta_o)$ . The center plot of figure 5 shows a cross section located approximately  $2.5\delta_o$  upstream of the SBLI shock crossing point. The downwash effect of the incident shock influences the flow in that corner, breaking the symmetry of the pair of corner vortices that was found further upstream. Only one vortex remains, which is located near the side-wall. The transverse flow pattern moves fluid downward and towards the center of the duct (positive  $z$  values). The remaining vortex, located near the side wall, represents an obstacle to the downward flow induced by the impinging shock, and it is thus pushed closer to the bottom wall. The right plot of figure 5 shows the recovery of the two counter-rotating vortices found at a station approximately  $6\delta_o$  downstream of the reflected SBLI shock-crossing point. Both the side- and bottom-wall boundary layers have thickened through the interaction with the shocks, and the vortex cores have lifted from each wall.

### CONCLUSIONS

Wall-modeled large-eddy simulations of the interaction of a shock wave and  $Re_\theta = 6,500$  turbulent boundary layers present in a nearly-square  $M = 2.05$  wind tunnel were validated through comparison with experimental PIV measurements. Two strengths of the reflected SBLI interaction were considered, resulting from an increasing height of the compression wedge that generates the incident shock wave.

Despite the equilibrium assumptions in the wall model, results from the simulations yielded accurate predictions of the non-equilibrium phenomena present in the flow (SBLI and presence of corner flows). This is attributed to the fact that the wall model is used in only a small fraction ( $\lesssim 10\%$ ) of the boundary layer, whereas the remaining ( $\gtrsim 90\%$ ) boundary layer turbulence is resolved. Thus, the outer part of the boundary layer responds to the adverse pressure gradient in the SBLI and the stress-induced secondary flows with LES accuracy; this outer-layer resolved information is then fed to the wall-model.

The simulation results were used to complement experimental findings regarding the three-dimensionality of the flow. Horizontal planes near the bottom wall are used to elucidate the distance over which the intensity of the interaction diminishes as the side walls are approached, and the curvature of the SBLI for each shock strength. Cross-sectional planes were used to describe the downstream evolution of corner flows near the bottom wall as influenced by

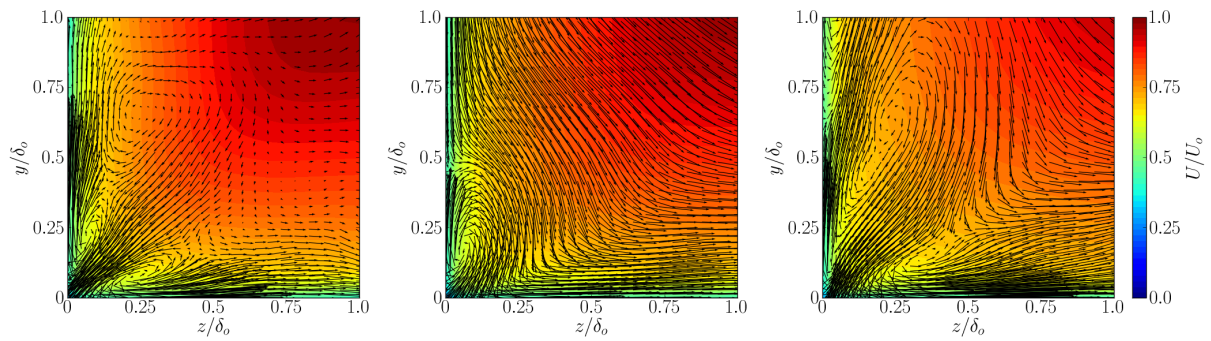


Figure 5. Downstream evolution of corner flows for the 1.1 mm-high wedge case near the corner  $y = z = 0$ , for stream-wise locations  $x/\delta_o = 1.9$  (left), 5.6 (center) and 14.8 (right). Contours: mean stream-wise velocity,  $U/U_o$ , arrows: the mean in-plane transverse velocity.

the impinging shock. The symmetry of the counter rotating vortex pair is broken by the downward motion induced by the incident shock, and later recovered downstream of the interaction.

Planned future work includes the study of a stronger SBLI configuration with a larger compression wedge meant to produce mean flow separation. This case will pose a more stringent test for the equilibrium wall model.

## ACKNOWLEDGMENTS

This work is supported by the United States Department of Energy under the Predictive Science Academic Alliance Program (PSAAP) at Stanford University. The authors acknowledge the following award for providing computing resources that have contributed to the research results here reported: "MRI-R2: Acquisition of a Hybrid CPU/GPU and Visualization Cluster for Multidisciplinary Studies in Transport Physics with Uncertainty Quantification." This award is funded under the American Recovery and Reinvestment Act of 2009 (Public Law 111-5, award number 960306).

## REFERENCES

- Bradshaw, P. 1987 Turbulent secondary flows. *Annu. Rev. Fluid Mech.* **19**, 53–74.
- Campo, L. M., Helmer, D. B. & Eaton, J. K. 2012 Validation experiment for shock boundary layer interactions: sensitivity to upstream geometric perturbations. *AIAA Paper 2012-1440*.
- Davis, D. O., Gessner, F. B. & Kerlick, G. D. 1986 Experimental and numerical investigation of supersonic turbulent flow through a square duct. *AIAA J.* **24** (1508).
- Dolling, D. S. 2001 Fifty years of shock-wave/boundary-layer interaction research: what next? *AIAA J.* **39**, 1517.
- Dupont, P., Haddad, C. & Debiève, J. 2006 Space and time organization in a shock-induced separated boundary layer. *J. Fluid. Mech.* **559**, 255–277.
- Dupont, P., Piponnier, S., Sidorenko, A. & Debive, J.F. 2008 Investigation by particle image velocimetry measurements of oblique shock reflection with separation. *AIAA J.* **48** (6), 1365–1370.
- Garnier, E., Sagaut, P. & Deville, M. 2002 Large eddy simulation of shock/boundary-layer interaction. *AIAA J.* **40** (10).
- Gessner, F. B. 1973 The origin of secondary flow in turbulent flow along a corner. *J. Fluid Mech.* **58**, 1–25.
- Gessner, F. B., Ferguson, S. D. & Lo, C. H. 1987 Experiments on supersonic turbulent flow development in a square duct. *AIAA J.* **25** (690).
- Grilli, M., Schmid, P. J., Hickel, S. & Adams, N. A. 2012 Analysis of unsteady behaviour in shockwave turbulent boundary layer interaction. *J. Fluid Mech.* **700**, 16–28.
- Helmer, D., Campo, L. & Eaton, J. 2012 Three-dimensional features of a Mach 2.1 shock/boundary layer interaction. *Exp. Fluids* **53**, 1347–1368.
- Humble, R., Elsinga, G., Scarano, F. & van Oudheusden, B. 2009 Three-dimensional instantaneous structure of a shock wave/turbulent boundary layer interaction. *J. of Fluid Mech.* **622**, 33–62.
- Kawai, S. & Larsson, J. 2012 Wall-modeling in large eddy simulation: length scales, grid resolution and accuracy. *Phys. Fluids* **24**, 15105.
- Klein, M., Sadiki, A. & Janicka, J. 2003 A digital filter based generation of inflow data for spatially developing direct numerical or large eddy simulations. *J. Comput. Phys.* **186**, 652–665.
- Pirozzoli, S. & Grasso, F. 2006 Direct numerical simulation of impinging shock wave/turbulent boundary layer interaction at  $M = 2.25$ . *J. Comput. Phys.* **18** (6), 065113.
- Pirozzoli, S., Larsson, J., Nichols, J. W., Bernardini, M., Morgan, B. E. & Lele, S. K. 2010 Analysis of unsteady effects in shock/boundary layer interactions. *CTR Annu. Res. Briefs* pp. 153–164.
- Priebe, S. & Pino Martin, M. 2012 Low-frequency unsteadiness in shock wave-turbulent boundary layer interaction. *J. Fluid Mech.* **699**, 1–49.
- Souverein, L., Dupont, P., Debieve, J., van Dussaugen, J., Oudheusden, B. & Scarano, F. 2010 Effect of interaction strength on unsteadiness in turbulent shock-wave-induced separations. *AIAA J.* **48**, 1480–1493.
- Touber, E. & Sandham, N. 2009 Large-eddy simulation of low-frequency unsteadiness in a turbulent shock-induced separation bubble. *Theor. Comput. Fluid Dyn.* **23**, 79–107.
- Vreman, A. W. 2004 An eddy-viscosity subgrid-scale model for turbulent shear flow: Algebraic theory and applications. *Phys. Fluids* **16** (10), 3670–3681.
- Wu, M. & Martin, M.P. 2008 Analysis of shockmotion in shockwave and turbulent boundary layer interaction using direct numerical simulation data. *J. Fluid Mech.* **594**, 71–83.